International Journal of Microwave and Wireless Technologies

cambridge.org/mrf

Research Paper

Cite this article: Do TNT, Bao M, He ZS, Hassona A, Kuylenstierna D, Zirath H (2019). A low-phase noise *D*-band signal source based on 130 nm SiGe BiCMOS and 0.15 μm AlGaN/GaN HEMT technologies. *International Journal of Microwave and Wireless Technologies* **11**, 456–465. https://doi.org/10.1017/S1759078719000291

Received: 23 November 2018
Revised: 18 February 2019
Accepted: 18 February 2019
First published online: 25 March 2019

Key words:
D-band; signal source; oscillator; GaN HEMT; frequency multiplier; amplifier; SiGe BiCMOS; low phase noise

Author for correspondence:
Thanh Ngoc Thi Do,
E-mail: tngoc@chalmers.se

© Cambridge University Press and the European Microwave Association 2019

CAMBRIDGE UNIVERSITY PRESS

A low-phase noise *D*-band signal source based on 130 nm SiGe BiCMOS and 0.15 μm AlGaN/GaN HEMT technologies

Thanh Ngoc Thi Do[1], Mingquan Bao[2], Zhongxia Simon He[1], Ahmed Hassona[1], Dan Kuylenstierna[1] and Herbert Zirath[1,2]

[1]Microwave Electronics Laboratory, Department of Microtechnology and Nanoscience, Chalmers University of Technology, Gothenburg, Sweden and [2]Ericsson Research, Ericsson AB, Gothenburg, Sweden

Abstract

This paper reports on a record-low-phase noise *D*-band signal source with 5 dBm output power, and 1.3 GHz tuning range. The source is based on the unconventional combination of a fundamental frequency 23 GHz oscillator in 150 nm AlGaN/GaN HEMT technology followed by a 130 nm SiGe BiCMOS MMIC including a sixtupler and an amplifier. The amplifier operates in compression mode as power-limiting amplifier, to equalize the source output power so that it is nearly independent of the oscillator's gate and drain bias voltages used for tuning the frequency of the source. The choice of using a GaN HEMT oscillator is motivated by the need for a low oscillator noise floor, which recently has been demonstrated as a bottleneck for data rates in wideband millimeter-wave communication systems. The phase noise performance of this signal source is −128 dBc/Hz at 10 MHz-offset. To the best of the authors' knowledge, this result is the lowest reported phase noise of *D*-band signal source.

Introduction

The ever-increasing data traffic in the society is constantly pushing the telecom infrastructure toward new innovations to increase network capacity [1, 2]. The capacity of a single communication channel may be increased by either larger bandwidth or improved spectral efficiency. The spectral efficiency that can be achieved is further limited by the signal-to-noise ratio of the communication channel [3]. Conventional frequency bands (up to 90 GHz) used today already address relatively advanced modulation formats and can be considered to be limited by bandwidth [4]. Naturally, the most promising pathway to increased data rates in the telecom infrastructure is to explore the large absolute bandwidth available at millimeter-wave frequencies.

In recent years, several high-data rate communication tests, deploying wideband signals beyond 100 GHz, have been demonstrated [5–7]. However, still none of these experiments have demonstrated simultaneously large bandwidth and high spectral efficiency [8]. To further increase the data rates of millimeter-wave communication systems, there is a need to support simultaneously large bandwidth and high orders of modulation. A challenge with wide communication channels is that they inevitably integrate more noise according to Nyquist's theorem. It has been proposed that the noise limiting the spectral efficiency in wideband millimeter-wave wireless communication systems is originating from the local oscillator (LO) and in particular the LO noise floor [8, 9]. Consequently, a key enabler for further increased data rates is low-noise millimeter-wave frequency sources.

To reach a low noise floor, a high signal-to-noise ratio is required. For this reason, a technology with high output power is beneficial. Consequently, short-gate length AlGaN/GaN HEMT technology has recently been proposed as a potential technology for low-phase noise millimeter-wave frequency generation thanks to high breakdown voltage [10, 11]. AlGaN/GaN HEMT is also by far the most potential technology for millimeter-wave power generation. On the other hand, III–V technologies, such as AlGaN/GaN HEMT, cannot compete with the integration levels of CMOS and BiCMOS technology. A Silicon technology will most likely be needed for the clock recovery. Further, good frequency multipliers and frequency converters have been demonstrated in SiGe HBT technology [12, 13]. In this perspective, a combination of AlGaN/GaN HEMT and BiCMOS technologies is a promising candidate for future high-end millimeter-wave wireless communication systems.

In this work, we demonstrate a *D*-band signal source combining 150 nm AlGaN/GaN HEMT technology from Qorvo and 130 nm SiGe BiCMOS technology from Infineon. The GaN HEMT technology is used for design of a Ka band fundamental-frequency oscillator and the SiGe HBT technology is used for design of a frequency sixtupler integrated with an amplifier. The oscillator, which is implemented as a reflection-type oscillator topology using a novel impedance-transformed tapped distributed resonator, demonstrates state-of-the-art

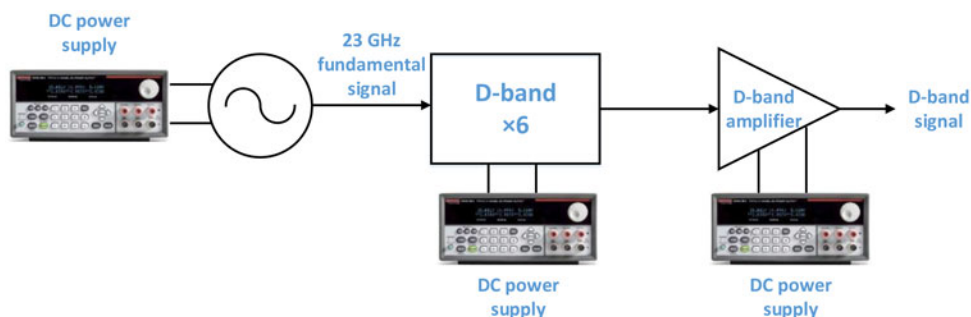

Fig. 1. Block diagram of the *D*-band signal source.

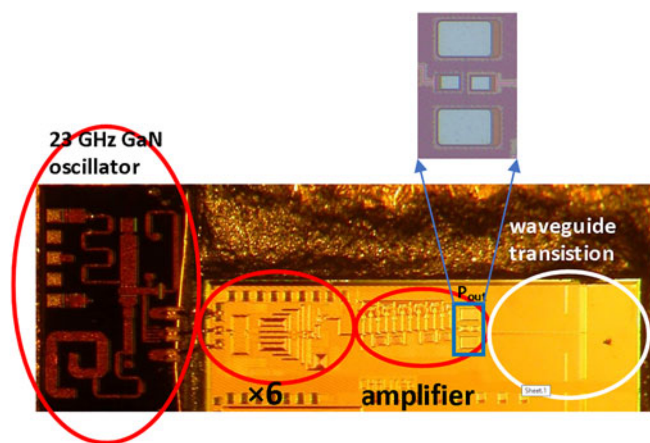

Fig. 2. Chip photo of the *D*-band signal source.

phase noise for a Ka band GaN HEMT oscillator. The oscillator is subsequently mounted and connected with bondwires to a SiGe HBT MMIC including the frequency sixtupler and the amplifier. The presented signal source demonstrates state-of-the-art phase noise of −128 dBc/Hz at 10 MHz off-set from a *D*-band carrier signal. It has a tuning range of 1.3 GHz (from 134.5 to 135.8 GHz) by varying the gate and drain bias voltages of the oscillator. The output power of the signal source is very constant around 5 dBm over the tuning range. To the best of the authors' knowledge, this is by far the best phase noise demonstrated for a *D*-band signal source. The circuit block design is presented in section 'Circuit block design'. Section 'Experimental results' shows measurement results and discussion. The conclusion is given in section 'Conclusion'.

Circuit block design

A block diagram of the *D*-band signal source is shown in Fig. 1. A sufficient RF input power for the sixtupler is generated by an oscillator operating at around 23 GHz. The sixtupler is subsequently followed by a wideband six-stage amplifier. The amplifier is driven in compression to equalize the *D*-band output power, which is nearly independent of the GaN oscillator's gate and drain voltages used for tuning the frequency of the source.

The oscillator is fabricated in Qorvo's 0.15 µm AlGaN/GaN HEMT technology with cut-off frequency (f_T) and maximum oscillation frequency (f_{max}) of 53 and 102.5 GHz, respectively, while the wideband sixtupler and amplifier are implemented in 130 nm SiGe BiCMOS technology with f_T and f_{max} of 250 and 370 GHz, respectively. Figure 2 shows the chip photo of the presented *D*-band source in which the GaN oscillator is wire-bonded to SiGe sixtupler and amplifier MMIC. This signal source not only has output RF probe for on-chip measurement, but also has an optional waveguide transition dedicated to bond-wire for future packaging as also seen in Fig. 2. The detailed description of each circuit in the block diagram is given as follow.

23 GHz GaN oscillator

The oscillator is based on reflection type oscillator topology (negative resistance oscillator) [14] in which the reflection amplifier is based on an integrated HEMT device (Q_1) with inductive termination at drain. The source of Q_1 is grounded through an inductor and a small resistance of 5 Ω for bias stabilization in parallel with a capacitor to peak the gain.

As mentioned in [14], the challenge in design of reflection-type oscillators is to optimize the coupling between the passive resonator and the active amplifier, i.e. the magnitude of the ratio between the resistive load of the resonator and the negative resistance of the reflection amplifier. The ratio cannot be fixed only by adjusting the gain of the reflection amplifier. It is desirable to have a sufficient amount of gain in the amplifier to make it less sensitive to gain variations which otherwise would translate into phase noise. For lowest phase noise, the resonator is designed for high *Q*, but also high impedance level to reach a resistance high enough to optimize the coupling factor.

Not all resonators can be tuned for impedance levels high enough to guarantee a simultaneously high resistance and quality factor. The work in [14] proposed a new type of resonator, a lumped parallel resonator transformed through a high-impedance $\lambda/4$ line. In this work, a similar transformed resonator is used, but with the difference that the lumped MIM capacitor is replaced with an open stub, see Fig. 3, which is more suitable at 23 GHz. To the best of the authors' knowledge, this type of fully distributed transformed tapped resonator has never been published before. By adjusting the tapping position and the width of the impedance transformer, a wide range of impedance conditions may be reached. Practical impedance values are limited by technology. In the chosen GaN HEMT MMIC technology, the characteristic impedance of the quarter-wave transformer (Z_t) can be about 70 Ω at highest and the characteristic impedance of the $\lambda/4$ resonator (Z_{res}) is about 35 Ω. The effective series

https://doi.org/10.1017/S1759078719000291 Published online by Cambridge University Press

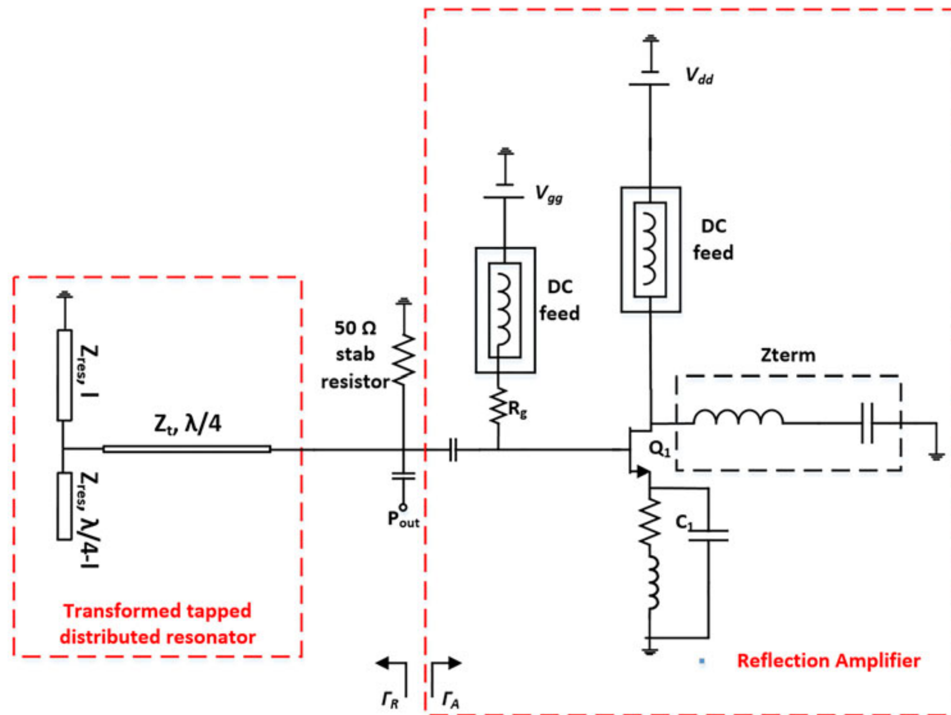

Fig. 3. Schematic representation of negative resistance GaN HEMT oscillator.

resistance at the resonant frequency can then be tuned from 2 to 50 Ω by changing the tapping position from $l = \lambda/8$ to $\lambda/32$. By tuning the length of the impedance transformer, the phase condition is met.

The circuit is designed in Keysight's Advanced Design System (ADS). The one-port *S*-parameters of the reflection amplifier are tuned to reach a reflection gain of 8 dB at 23 GHz, corresponding to a reflection coefficient of $\Gamma_A = -2.5$ or a negative resistance of $R_A = -21\ \Omega$.

The resonator is tuned for optimum phase noise and sufficient gain margin. The final oscillator shown in Fig. 2 has a total loop gain of 3 dB, corresponding to a reflection loss of 5 dB for the passive resonator which is obtained for a quarter-wave transformer impedance of $Z_t = 71\ \Omega$ and a tune-length of $l = \lambda/8$. EM-simulations of the designed resonator reveals an unloaded quality factor of $Q = 27$, which is good for an integrated MMIC oscillator at 23 GHz. In the schematic representation of this negative resistance oscillator, a 50 Ω load is added in parallel with the resonator to suppress unwanted resonance out-of-band oscillations without affecting the fundamental oscillation frequency. The gate bias voltage is injected through a gate resistance of 900 Ω while the drain voltage is biased through a drain bias transmission line. The power is coupled out from a small interdigital capacitor of effective capacitance 0.05 pF. The chip photo is shown in Fig. 2.

D-*band SiGe sixtupler*

The schematic representation of the sixtupler is shown in Fig. 4. It consists of a balanced frequency tripler, followed by a buffer amplifier, a differential frequency doubler and a two-stage power amplifiers. First, the single-ended input signal is transformed into a differential signal in an on-chip balun. In principle, transistors Q_1s will generate harmonics and cascaded transistors, Q_2s, will mix the first and the second harmonics in the frequency tripler to produce the third harmonic. The frequency tripler has a differential output in which the odd-order harmonics can be amplified in differential mode while even-order harmonics, will be suppressed in the common-mode through the buffer amplifier. Then, the output signal of the buffer amplifier will pass through a differential frequency doubler consisting of a transistor pair, Q_4s. The collectors of the transistors Q_4s are connected where the differential odd-harmonics are cancelled while even-harmonics are constructively added. Finally, a two-stage power amplifier stage increases the output power for the sixtupler chain. The first stage is made up of a transistor, Q_5, while the second stage consists of two transistors, Q_6s, connected in parallel. It should be mentioned that between individual blocks, i.e. tripler, buffer amplifier, doubler, and power amplifier, inter-stage matching networks are also designed. In each design, harmonics (up to the sixth order) at output are simulated using harmonic balance algorithm. The transistors' size, biases, and the parameters of the passive components, i.e. capacitances, the length of the transmission line, etc., are chosen from the optimization with the targets of wideband, high output power, and efficiency. The circuit is designed with Cadence. In the final design simulation, transmission line/capacitor models from the design kit are replaced by EM models obtained from the Sonnet simulator to reach highest accuracy in simulation.

The SiGe BiCMOS process used provides six metal layers which are named as *M1*, *M2…M6* from bottom to top metal layers. In this work, the metal layer 4 (*M4*) is used for the ground plane and the top metal layer (*M6*) is used for transmission lines. All transmission lines have a width of 5 μm with different lengths. The broad-side-coupled transmission line in *M6* and *M5* are used to build a balun. The coupled lines are folded, occupying an area

https://doi.org/10.1017/S1759078719000291 Published online by Cambridge University Press

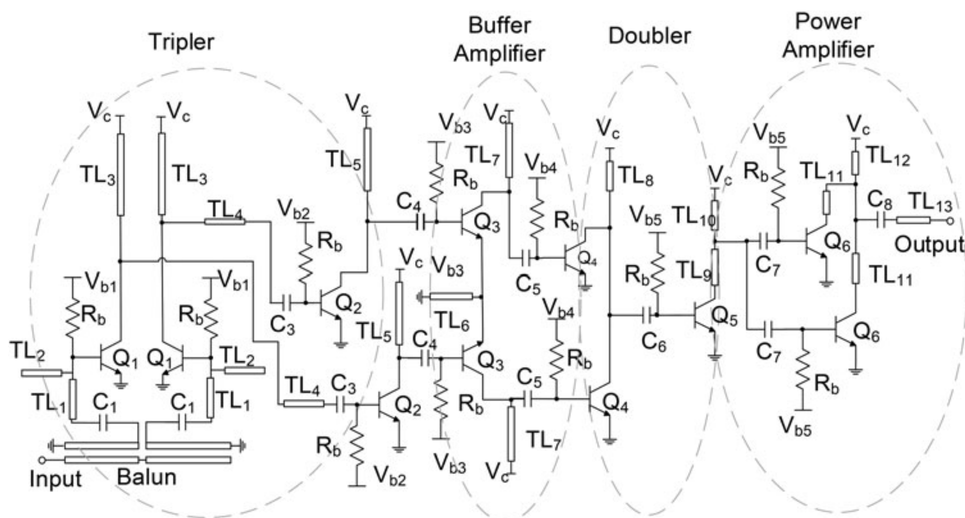

Fig. 4. Schematic representation of *D*-band SiGe sixtupler.

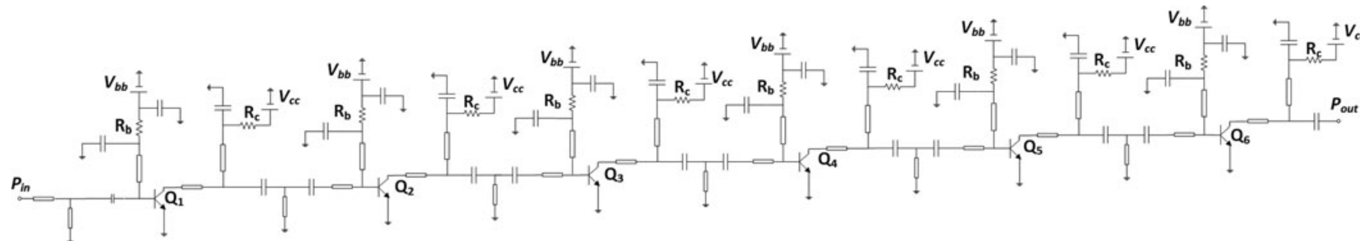

Fig. 5. Schematic representation of *D*-band SiGe amplifier.

of 127 μm × 283 μm. The metal–insulator–metal (MIM) capacitors provided by the foundry are used. Transistors Q_1 and Q_2 have two emitter fingers with a length of 6.3 μm each. The other transistors have a single emitter finger with a length of 10 μm. The chip photo is shown in Fig. 2.

D-band SiGe amplifier

Figure 5 shows the schematic representation of the designed amplifier. It consists of six cascaded stages common-emitter amplifier in order to achieve a sufficient amount of gain to get saturation for a given input. The matching networks are also designed to optimize the gain and the matching between stages. The lossy-matching concept employing the resistive loaded stub is used at each stage of the amplifier to achieve a large bandwidth. Moreover, the number of biases in this design is reduced to 2: one for the bases and one for the collectors for the six stages to increase the usability. All bases and collectors are biased through resistors of 200 and 10 Ω, respectively. All transmission lines have a width of 4.9 μm with different lengths. All transistors have an emitter length of 4 μm. The chip photo is shown in Fig. 2.

Experimental results

Each circuit in the presented signal source has been fabricated also as sub-blocks. This section presents measurement set-ups and performance of the complete signal source as well as for each sub-block function.

Oscillator measurements

The designed 23 GHz GaN HEMT oscillator is characterized on-chip using an FSUP50 signal-source analyzer from Rohde & Schwarz. The gate and drain bias voltages are controlled from a Keithley power supply.

Figure 6 shows the oscillation frequency versus the gate biasing with drain bias voltage as a parameter. The oscillation frequency is shifted down about 4% compared with the simulated result (23.5 GHz). The output power is varied from −11 to 4.5 dBm for all swept bias points, see Fig. 7. With 4 dBm maximum output power, the GaN oscillator is sufficient to drive the sixtupler. Figure 10 presents the measured phase noise versus offset frequency. The lowest measured phase noise at 100 kHz and 1 MHz off-set is −99 dBc/Hz and −129 dBc/Hz, respectively, at V_{dd} = 5 V and V_{gg} = −1.4 V. The red dashed ellipse in Fig. 7 indicates the drain voltage giving the best phase noise. Table 1 shows the comparison of this GaN oscillator to other state-of-the-art MMIC III–V oscillators reported in open literature. It can be seen that the designed oscillator are in line with the state-of-the-art MMIC GaN HEMT oscillators considering operating frequency and 1 MHz phase noise performance. The normalized phase noise at 1 MHz offset of this oscillator is also comparable with the state-of-the-art MMIC InGaP HBT-based oscillators [20] for comparable frequency.

Sixtupler measurements

The sixtupler is characterized on-chip. Powers of different harmonics are measured by a PNA-X Network Analyzer (N5247A) from

https://doi.org/10.1017/S1759078719000291 Published online by Cambridge University Press

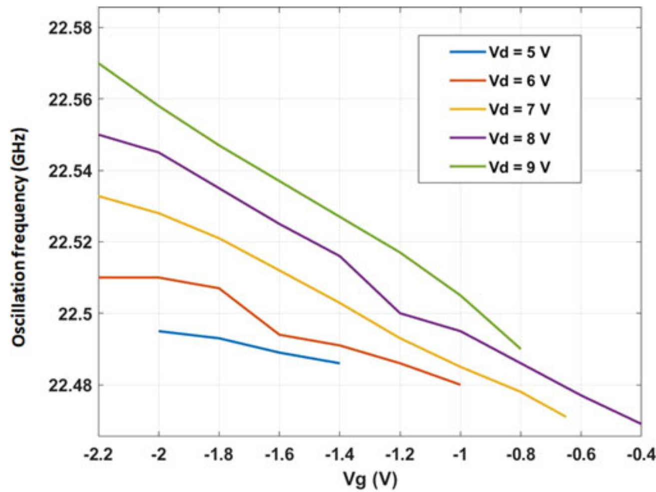

Fig. 6. Oscillating frequency of the GaN HEMT oscillator at different drain bias voltages versus the gate bias voltage.

Table 1. Comparison to other state-of-the-art MMIC III–V oscillators

Ref.	Process	f_o (GHz)	P_{out} (dBm)	Min PN at 1 MHz	Normalized PN[a] at 1 MHz
[15]	GaN HEMT	9.1	6	−130	209
[16]	GaN HEMT	9.9	17	−135[b]	215
[11]	GaN HEMT	9.92	−6	−136	216
[17]	GaN HEMT	15.05	−6	−133	216
[18]	GaN HEMT	12.3	5	−127	209
[19]	GaN HEMT	7.9	21	−135	213
[20]	InGaP HBT	25	−1	−130	218
[21]	InGaP HBT	6.4	5.5	−138	214
[22]	InGaP HBT	8.9	7	−128	208
This work	GaN HEMT	22.5	1	−129	216

[a]Normalized phase noise = $-\pounds(f_m) + 20\log10(f_o/f_m)$ where $\pounds(f_m)$ is the phase noise at offset frequency f_m, f_o is the oscillation frequency.
[b]Extrapolated by 30 dB/decade.

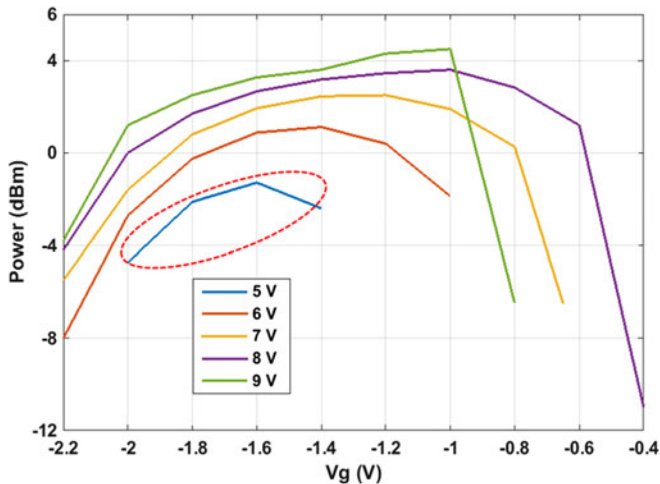

Fig. 7. Output power of the GaN HEMT oscillator at different drain bias voltages versus the gate bias voltage.

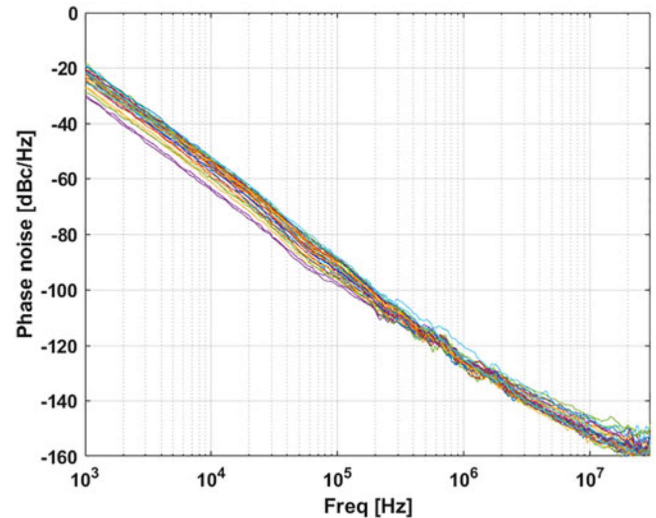

Fig. 8. Measured phase noise versus offset frequency for the GaN HEMT oscillator.

Keysight. WR-10 and WR-6.5 extenders from Virginia Diodes, Inc. are used for *W*-band and *D*-band measurements, respectively. Two four-channel programmable power supplies from Rohde & Schwarz HAMEG are used for DC biasing.

Figure 9 shows the power of the fifth, the sixth, and the seventh harmonics versus the output frequency (f_{out}) of the sixtupler, corresponding to the frequency of the input signal from 18.3 to 28.3 GHz (f_{out}/6) and the fixed input power of 4.4 dBm. As shown in Fig. 9, the maximum output power is 4.5 dBm and the 3 dB bandwidth is 29 GHz (from 115 to 144 GHz). The rejection of the undesired fifth and seventh harmonics is larger than 10 dBc.

Figure 10 shows the output power and the power efficiency of the sixtupler versus the input power. The sixtupler consumes DC power of 310 mW. The maximum power efficiency is 0.9%. It can be seen that output powers get saturated at frequencies of 110, 120, 130, and 140 GHz when the input power is larger than 3 dBm. On top, the sixtupler exhibits a wide frequency bandwidth, a high output power in comparison with other frequency multipliers (i.e. ×4, ×6, ×8) utilizing SiGe technology [12, 23–25].

Amplifier measurements

The amplifier is also measured on-chip by a PNA-X Network Analyzer (N5247A) from Keysight and WR-6.5 extenders from Virginia Diodes, Inc. DC power supply from Rohde & Schwarz HAMEG is used for DC biasing.

Figure 11 shows the measured small signal *S*-parameters. The six-stage amplifier has a maximum small signal gain (S_{21}) of nearly 20 dB and a 3 dB bandwidth from 115 to 149 GHz. Over the whole *D*-band, the small signal gain is better than 10 dB and reflection coefficient at the input (S_{11}) and output (S_{22}) are lower than −6 and −10 dB, respectively. It should be noted that input power was reduced to −40 dBm to avoid amplifier saturation. For this reason, $|S_{11}|$ is more noisy compared with $|S_{22}|$.

Figure 12 shows the measured conversion gain at 130, 140, and 150 GHz, respectively, when the input power is swept from −40 to 0 dBm. It can be seen that output gains get saturated at input power of −5 dBm for 130 and 140 GHz. The amplifier consumes DC power of 92 mW.

https://doi.org/10.1017/S1759078719000291 Published online by Cambridge University Press

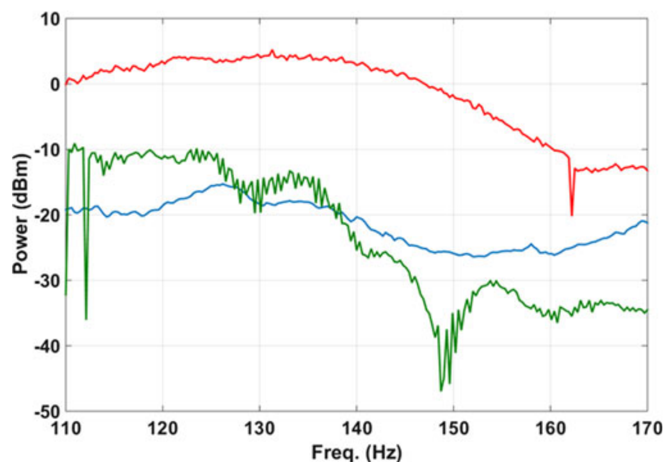

Fig. 9. Measured output power of the sixtupler versus output frequency.

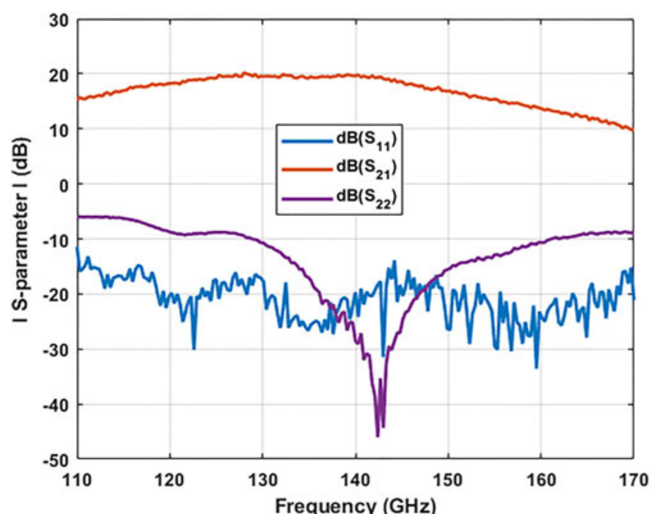

Fig. 11. Measured *S*-parameters versus frequencies.

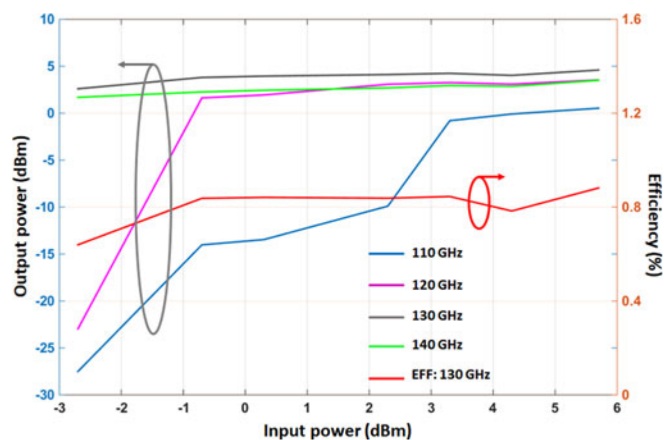

Fig. 10. Output powers at 110, 120, 130, and 140 GHz, as well as the power efficiency at 130 GHz versus input power.

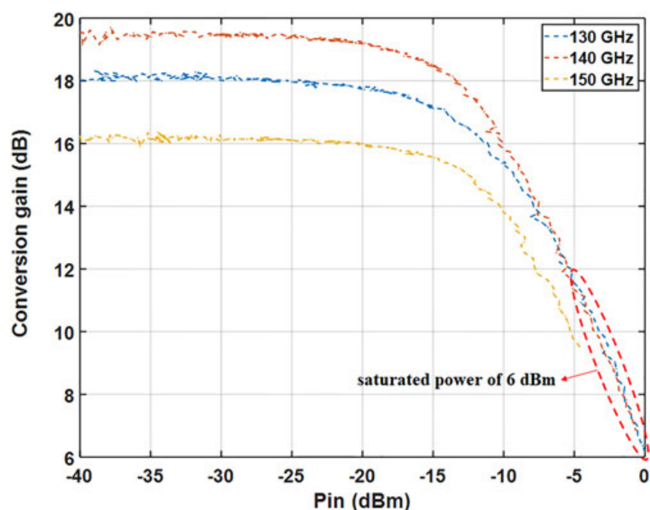

Fig. 12. Measured conversion gain at 130, 140, and 150 GHz, respectively, when the input power is swept from −40 to 0 dBm.

Signal source performance

The signal source is characterized on-wafer using an FSUP50 signal-source analyzer from Rohde & Schwarz. The frequency range of the FSUP is extended using an external *D*-band sub-harmonic mixer according to the measurement set-up in Fig. 13. A *D*-band fixed attenuator of 12 dB is also used in the setup, avoiding the power saturation due to external mixer. The total loss from attenuator, *D*-band probe and coaxial connection was characterized to be 14 dB.

Figure 14 presents the measured output spectrum from R&S FSUP in the whole *D*-band. It shows that *D*-band signals at around 135 GHz with output power about 5 dBm (after correction for probe and attenuator losses) are generated from the designed signal source. The harmonics suppression is better than 20 dB. Figure 15 presents output power of the designed signal source versus gate bias voltage of the GaN oscillator while drain bias voltage of the GaN oscillator (5 V) and other biases are fixed at optimum points. The output power of the signal source is almost constant about 5 dBm over different oscillator's gate bias voltages, which is reasonable when considering the input–output power of the amplifier that is about 6 dBm. It should be noted that the amplifier operates in compression mode, see the red dashed ellipse in Fig. 12, to equalize the source output power so that it is nearly independent of the oscillator's gate and drain bias voltages used for tuning the source frequency. The small difference may be due to mismatch, losses in bond-wires, and sample-to-sample variations. A bandwidth of 1.3 GHz (from 134.5 to 135.8 GHz) can be achieved by tuning the GaN oscillator's gate and drain bias voltages. The total DC power consumption of the signal source varies from 528 mW to 2.12 W over the tuning range.

Accurate phase noise characterizing of free-running millimeter-wave sources is not trivial. It generally requires some kind of phase stabilization, e.g. the PLL method or the discriminator method [26]. Off-the-shelf systems compatible with these methods beyond 100 GHz are rarely available. Instead phase noise is normally determined using the spectrum-analyzer method, i.e. reading directly from the measured spectrum. Modern commercial spectrum analyzers have automatic routines for stepping the frequency and adjusting the resolution bandwidth

https://doi.org/10.1017/S1759078719000291 Published online by Cambridge University Press

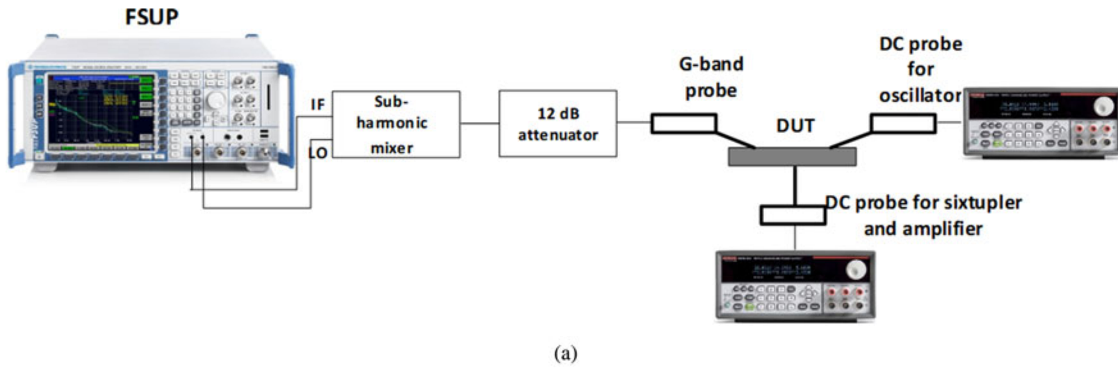

(a)

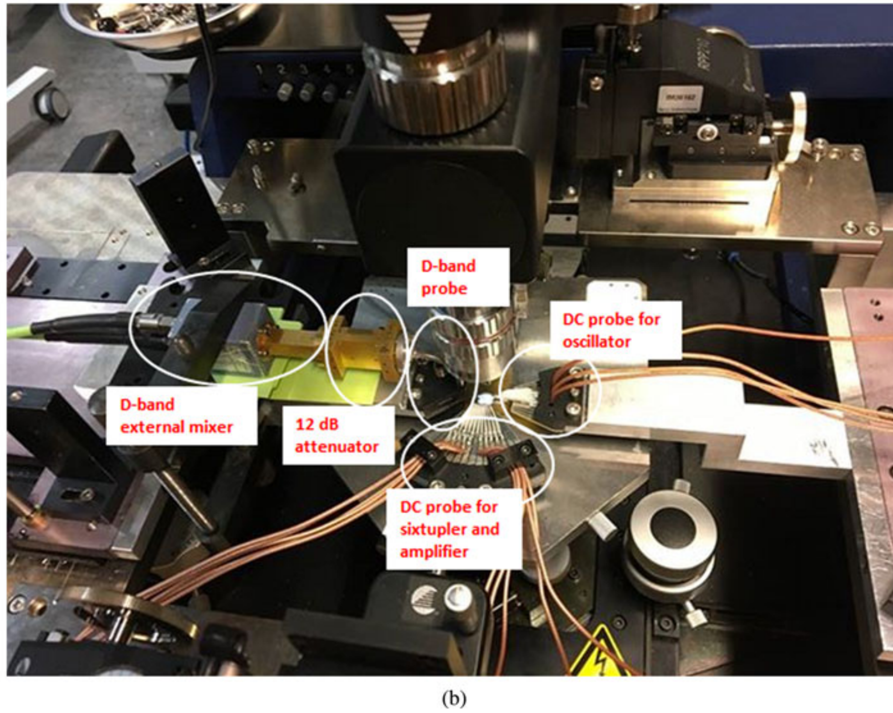

(b)

Fig. 13. Signal source measurement setup. (a) Block diagram. (b) On-wafer test setup.

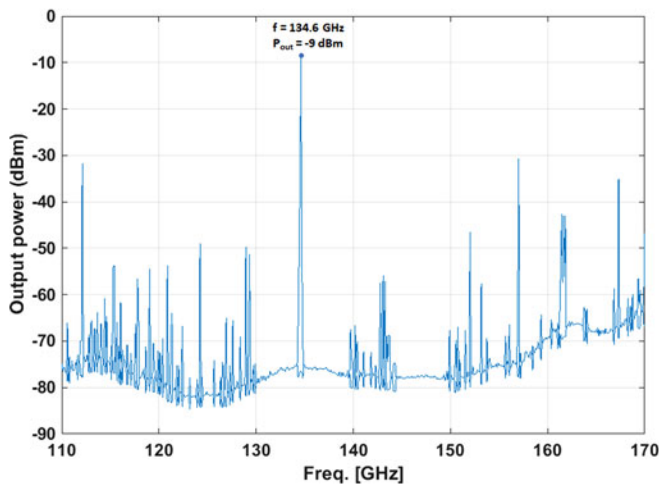

Fig. 14. Measured output spectrum from FSUP in *D*-band.

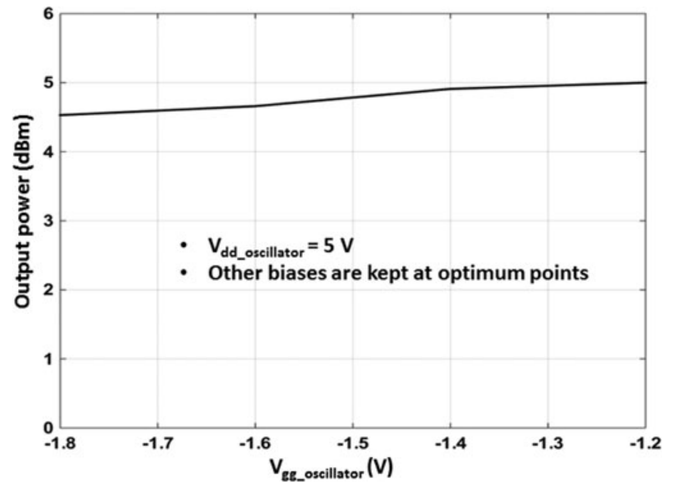

Fig. 15. Measured output power of the presented signal source versus different gate bias voltages of the GaN oscillator (V_{dd_osc} = 8 V and other biases are fixed at the optimum points).

https://doi.org/10.1017/S1759078719000291 Published online by Cambridge University Press

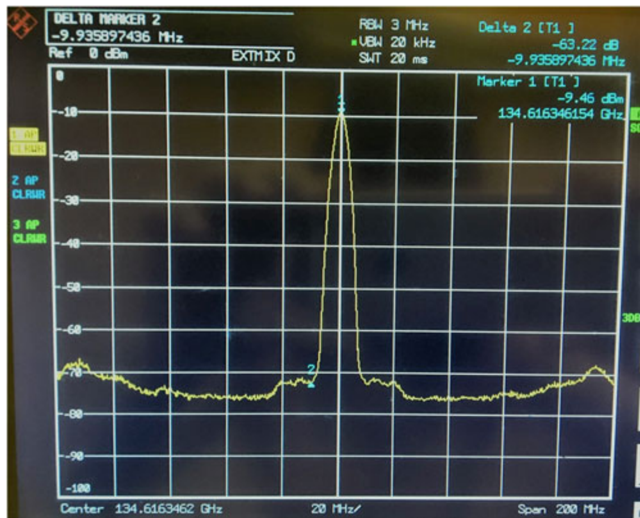

Fig. 16. Measured output spectrum from FSUP with frequency span of 200 MHz at $V_{gg_osc} = -1.8$ V, $V_{dd_osc} = 5$ V, other biases are fixed at optimum points (noted that a 12 dB attenuation and 2 dB probe loss should be added to measured power).

to synthesize the phase noise spectrum versus off-set frequency. The R&S FSUP signal source analyzer used in this work has a dedicated hardware option using cross-correlation of two PLLs to reach a very low noise floor (https://cdn.rohde-schwarz.com/pws/dl_downloads/dl_common_library/dl_brochures_and_data-sheets/ pdf_1/FSUP_dat-sw_en.pdf). This method is however not compatible with the external mixers needed to characterize *D*-band oscillators. For *D*-band frequencies, the remaining options for phase noise characterization are to either use a spectrum-based phase noise routine, or to manually adjust frequency span and resolution bandwidth to be able to estimate phase noise from the measured spectrum. In this work, the latter approach is addressed since the automatic routine gave erroneous results due to spurs and long-term drift of the signal.

Figure 16 shows measured spectra for the signal source at $V_{gg_osc} = -1.8$ V, $V_{dd_osc} = 5$ V, other biases are fixed at optimum points that gives the best phase noise. The single-side band phase noise (SSB) can be calculated from the measured power spectral density normalized to the resolution bandwidth, i.e.

$$\mathcal{L}(\Delta f) = P_n(RBW) - P_s - 10 \times \log_{10}(RBW), \quad (1)$$

where P_s is the carrier signal power and P_n is the noise power within the resolution bandwidth (RBW) at offset Δf.

The used RBW is a trade-off between noise floor and resolution. RBW cannot be chosen higher than the lowest offset frequency for characterization of phase noise. Despite lowering the noise floor, the RBW has little effect on the sample-to-sample variations, which may be lowered by adjusting the video bandwidth, acting as a low-pass filter or floating mean smoothing function [27].

From the spectrum in Fig. 17 the measured phase noise at an off-set frequency of 10 MHz can be estimated to about −128 dBc/Hz at 10 MHz offset frequency. The estimated phase noise can be compared with the phase noise of the 23 GHz oscillator which was measured to −155 dBc/Hz for the same off-set and bias point, corresponding to a residual phase of 17 dB for the frequency sixtupler, which is more or less in line with the theoretical $20\log_{10}(6) = 15.6$ dB. As mentioned in the introduction, a particular motivation for using a GaN HEMT oscillator in the signal source is to reach a low wideband noise for high-data rate millimeter-wave communication. The spectrum in Fig. 16 shows a noise floor on the order of −130 dBc/Hz. However, this noise floor is likely limited by the measurement set-up. The FSUP spectrum analyzer has a noise floor about −165 dBc/Hz which is degraded to −130 dBc/Hz considering the conversion loss of the harmonic mixers (23 dB) and the 12 dB attenuation used.

Table 2 compares the performance of millimeter-wave signal sources in *D*-band using SiGe Bipolar and CMOS Technologies reported in open literature. Each of them has different topologies

Table 2. Summary of signal sources using Bipolar and CMOS Technologies in D-band (110–170 GHz)

Ref.	Process/f_T/f_{max}	Architecture	f_o (GHz)	P_{out} (dBm)	BW (GHz)	PN at 1 MHz	PN at 10 MHz
[28]	0.13 μm SiGe BiCMOS/260/380	VCO + Tripler + Amp	160	5	7	−80[a]	–
[29]	0.13 μm SiGe BiCMOS/-/135	Fundamental OSC	121	−3.5	0	−88	−102
[29]	0.13 μm SiGe BiCMOS/-/135	Fundamental OSC	104	−2.7	0	−93.3	−105
[30]	Infineon's 0.35 μm B7HF200/170/250	VCO + Doubler	144	3	39	−93	–
[31]	0.18 μm BiCMOS Technology	Osc + Amp + Doubler	133	3	0	–	−107.2
[32]	SiGe HBT/270/340	Push-push (second harmonic) osc + Amp	165	−3.5	0	–	−104[a]
[33]	SiGe HBT/300/450	Fundamental OSC	154	7	0	−87	–
[34]	SiGe/225/320	VCO + Amp	122	2	16	−95	−115
[35]	SiGe/170/250	VCO + Gilbert-Doubler	148	3	46	−94	–
This work	0.13 μm BiCMOS /250/370 + 0.15 μm AlGaN/GaN HEMT	Osc + Sixtupler + Amp	135	5	1.3	−112[b]	−128[c]

[a]Extrapolated using 20log(*N*).
[b]Estimated from residual phase noise at 10 MHz off-set.
[c]May be limited by noise floor of measurement system.

https://doi.org/10.1017/S1759078719000291 Published online by Cambridge University Press

as well as transistor technologies. It is found that the presented signal source has high output power and the best phase noise.

Conclusion

A low-phase noise *D*-band signal source at around 135 GHz consisting of an unconventional combination of a fundamental frequency 23 GHz GaN HEMT oscillator and a SiGe BiCMOS MMIC sixtupler and amplifier is reported. The presented signal source has a nearly constant output power of 5 dBm with a tuning range of 1.3 GHz. The aim of using a GaN HEMT oscillator in the signal source is to reach a low noise floor which is critical for high-data rate millimeter-wave communication. The designed GaN HEMT oscillator is based on a novel transformed tapped distributed resonator and presents phase noise better than any previously reported GaN HEMT oscillator at the same frequency. Together with the state-of-the-art SiGe HBT sixtupler with low residual phase noise, it enables state-of-the-art *D*-band signal source performance. The phase noise performance at 10 MHz offset from a 135 GHz carrier is −128 dBc/Hz.

Acknowledgement. Infineon Technologies and Qorvo Technologies are acknowledged for fabricating the circuits. This work was financed by the European Union's Horizon 2020 research and innovation program under grant agreement no. 644039.

References

1. **Webb W** (2007) *Wireless Communications: The Future, UK*. Chichester: Wiley.
2. **Cherry S** (2004) Edholm's law of bandwidth – telecommunications data rates are as predictable as Moore's law. *IEEE Spectrum* **41**, 58–60.
3. **Shannon CE** (1949) Communication theory of secrecy systems. *The Bell System Tech. J.* **28**, 656–715.
4. **Chen J, He Z, Kuylenstierna D, Eriksson T, Hörberg M, Swahn T and Zirath H** (2017) Does LO noise floor limit performance in multi-gigabit millimetre-wave communication? *IEEE Microwave and Wireless Components Letters* **27**, 769–771.
5. **Grzyb J, Vazquez PR, Heinemann B and Pfeiffer UR** (2018) A high-speed QPSK/16-QAM 1 m Wireless Link with Tunable 220–260 GHz LO Carrier in SiGe HBT Technology, 43rd International Conference on Infrared, Millimeter, and Terahertz waves (IRMMW-THz), Nagoya.
6. **Carpenter S, He ZS and Zirath H** (2018) Multi-functional D-band I/Q modulator/demodulator MMICs in SiGe BiCMOS technology. *International Journal of Microwave and Wireless Technologies* **10**, 596–604.
7. **Eissa MH, Malignaggi A, Wang R, Elkhouly M, Schmalz K, Ulusoy AC and Kissinger D** (2018) Wideband 240 GHz transmitter and receiver in BiCMOS technology with 25-Gbit/s data rate. *IEEE Journal of Solid-State Circuits* **53**, 2532–2542.
8. **Chen J, He Z, Kuylenstierna D, Gunnarsson SE, Eriksson T, Swahn T and Zirath H** (2018) Influence of white LO noise on wideband communication. *IEEE Transactions on Microwave Theory and Techniques* **66**, 3349–3359.
9. **Antes J and Kallfass I** (2015) Performance estimation for broadband multi-gigabit millimeter- and sub-millimeter-wave wireless communication links. *IEEE Transactions on Microwave Theory and Techniques* **63**, 3288–3299.
10. **Liu H, Zhu X, Boon CC, Yi X, Mao M and Yang W** (2014) Design of ultra-low phase noise and high power integrated oscillator in 0.25 μm GaN-on-SiC HEMT technology. *IEEE Microwave and Wireless Components Letters* **24**, 120–122.
11. **Lai S, Kuylenstierna D, Özen M, Hörberg M, Rorsman N, Angelov I and Zirath H** (2014) Low phase noise GaN HEMT oscillators with excellent figures of merit. *IEEE Microwave Components Letter* **24**, 412–414.
12. **Yuan S and Schumacher H** (2013) A SiGe:C BiCMOS 140 GHz wideband frequency multiplier-by-8 with differential output, IEEE European Microwave Integrated Circuits Conference (EuMIC), Nuremberg.
13. **Carpenter S, He Z and Zirath H** (2017) A direct carrier I/Q modulator for high-speed communication at D-band using 130 nm SiGe BiCMOS technology, IEEE European Microwave Integrated Circuits Conference (EuMIC), Nuremberg.
14. **Lenk F, Schott M, Hilsenbeck J and Heinrich W** (2014) A new design approach for low phase noise reflection-type MMIC oscillators. *IEEE Transactions on Microwave Theory and Techniques* **52**, 2725–2731.
15. **Lai S, Kuylenstierna D, Hörberg M, Rorsman N, Angelov I, Andersson K and Zirath H** (2013) Accurate phase noise prediction for a balanced colpitts GaN HEMT MMIC Oscillators. *IEEE Transactions on Microwave Theory and Techniques* **61**, 3916–3926.
16. **Soubercaze-Pun S, Tartarin JG, Bary L, Rayssac J, Morvan E, Grimbert B, Delage SL, De Jeager J-C and Graffeuil J** (2006) Design of a X-band GaN Oscillator: From the low frequency noise device characterization and large signal modeling to circuit design, International Microwave Symposium Digest, San Francisco.
17. **Hörberg M and Kuylenstierna D** (2015) Low phase noise power-efficient MMIC GaN HEMT Oscillator at 15 GHz based on a Quasi-lumped on chip resonator, IEEE MTT-S International Microwave Symposium Digest, Arizona.
18. **Do TNT, Hörberg M, Lai S, Wollersjo S-H, Johansson D, Zirath H and Kuylenstierna D** (2017) 7-13 GHz MMIC GaN HEMT Voltage-Controlled-Oscillators (VCOs) for satellite applications, IEEE European Microwave Integrated Circuits Conference (EuMIC), Nuremberg.
19. **Liu H, Zhu X, Boon C-C, Yi X, Mao M and Yang W** (2014) Design of ultra-low phase noise and high power integrated oscillator in 0.25 μm GaN-on-SiC HEMT technology. *IEEE Microwave Components Letter* **24**, 120–122.
20. **Bao M, Li Y and Jacobsson H** (2005) A 25-GHz ultra-low phase noise InGaP/GaAs HBT VCO. *IEEE Microwave Components Letter* **15**, 751–753.
21. **Zirath H, Kozhuharov R and Ferndahl M** (2005) Balanced Colpitts-oscillator MMICs designed for ultra-low phase noise. *IEEE Journal of Solid-State Circuits* **40**, 2077–2086.
22. **Kuylenstierna D, Lai S, Mingquan B and Zirath H** (2012) Design of low-phase-noise oscillators and wideband VCOs in InGaP-HBT technology. *IEEE Transactions on Microwave Theory and Techniques* **60**, 3420–3430.
23. **Ergintav A, Herzel F, Borngraber J, Kissinger D and Ng HJ** (2017) An integrated 240 GHz differential frequency sixtupler in SiGe BiCMOS technology, IEEE 17th Topical Meeting on Silicon Monolithic Integrated Circuits in RF Systems (SiRF), Arizona.
24. **Wang Y, Goh WL and Zhong Xiong Y** (2012) A 9% Power Efficiency 121-to-137 GHz Phase-Controlled Push-Push Frequency Quadrupler in 0.13 μm SiGe BiCMOS, IEEE Solid-State Circuits Conf., San Francisco.
25. **Kucharski M, Malignaggi A, Kissinger D and Jalli Ng H** (2017) A wideband 129–171 GHz frequency quadrupler using a stacked Bootstrapped Gilbert cell in 0.13 μm SiGe BiCMOS", IEEE Bipolar/BiCMOS Circuits and Technology Meeting (BCTM).
26. **Keysight Technologies: Phase Noise Measurement Methods and Techniques**, https://www.keysight.com/upload/cmc_upload/All/PhaseNoise_webcast_19Jul12.pdf.
27. **Keysight Technologies: Spectrum Analysis Basic – Application Note 150**, http://literature.cdn.keysight.com/litweb/pdf/5952-0292.pdf
28. **Pfeiffer UR, Ojefors E and Zhao Y** (2010) A SiGe quadrature transmitter and receiver chipset for emerging high-frequency applications at 160 GHz, IEEE Int. Solid-State Circuits Conf., San Francisco.
29. **Momeni O and Afshari E** (2011) High power terahertz and millimeter-wave oscillator design: a systematic approach. *IEEE Journal of Solid-State Circuits* **46**, 583–597.
30. **Bredendiek C, Pohl N, Aufinger K and Bilgic A** (2012) An Ultra-Wideband D-band Signal Source Chip Using a Fundamental VCO with Frequency Doubler in a SiGe Bipolar Technology, IEEE Radio Frequency Integrated Circuits Symposium, Montreal.
31. **Jung S, Yn J and Rieh J-S** (2015) A D-band Signal source based on SiGe 0.18 μm BiCMOS Technology. *Journal of Electromagnetic Engineering and Science* **15**, 232–238.
32. **Laskin E, Chevalier P, Chantre A, Sautreuil B and Voinigescu SP** (2008) 165-GHz transceiver in SiGe technology. *IEEE Journal of Solid-State Circuits* **43**, 1087–1100.

https://doi.org/10.1017/S1759078719000291 Published online by Cambridge University Press

33. **Zeinolabedinzadeh S, Song P, Kaynak M, Kamarei M, Tillack B and Cressler JD** (2014) Low Phase Noise and High Output Power 367 GHz and 154 GHz Signal Sources in 130 nm SiGe HBT Technology, IEEE MTT-S International Microwave Symposium, Florida.
34. **Jahn M, Knapp H and Stelzer A** (2011) A 122-GHz SiGe-based signal-generation chip employing a fundamental-wave oscillator with capacitive feedback frequency-enhancement. *IEEE Journal of Solid-State Circuits* **46**, 2009–2020.
35. **Jaeschke T, Bredendiek C, Kuppers S and Pohl N** (2014) High-precision D-band FMCW-radar sensor based on a wideband SiGe-transceiver MMIC. *IEEE Transactions on Microwave Theory and Techniques* **62** 3582–3597.

Thanh Ngoc Thi Do received the M.S. degree in Electrical Engineering from Chalmers University of Technology in 2011 and is currently working toward the Ph.D. degree at Chalmers University of Technology. She is currently with the Microwave Electronics Laboratory, Chalmers University of Technology. Her research interests are MMIC designs in different transistor technologies such as GaN HEMTs, InP HBTs, SiGe HBTs, low-phase noise frequency generation and low-frequency noise characterization.

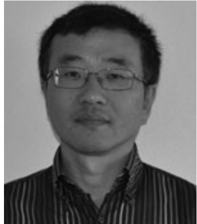

Mingquan Bao received the B.S. and M.S. degrees in Electrical Engineering from Zhejiang University, Hangzhou, China, in 1985 and 1988, respectively, and the Ph.D. degree in Radar Remote Sensing from the University of Hamburg, Hamburg, Germany, in 1995. From 1995 to 1997, he was with the Institute of Oceanography, University of Hamburg. From 1997 to 2000, he was with the Center for Remote Imaging Sensing and Processing, University of Singapore, Singapore. From 2000 to 2001, he was with the German Aerospace Center (DLR), Germany. Since 2001, he has been with Microwave System, Radio Access Technologies, Ericsson Research, Ericsson AB, Gothenburg, Sweden. He has authored over 50 papers in refereed journals and conferences. He holds 40 US, European, Japan, and China patents. His research interests include RF integrated circuit (RFIC) designs such as LNAs, mixers, frequency multipliers, power detectors, and VCOs in silicon, InP, GaAs, GaN technologies.

Zhongxia Simon He (M'09) received the M.Sc. degree from Beijing Institute of Technology, Beijing, China, and the Ph.D. degree from Chalmers University of Technology, Göteborg, Sweden, in 2008 and 2014, respectively. He is currently an Assistant Professor with the Microwave Electronics Laboratory, Department of Microtechnology and Nanoscience (MC2), Chalmers University. His current research interests include high data rate wireless communication, modulation and demodulation, mixed-signal integrated circuit design, radar, and packaging.

Ahmed Hassona received his B.Sc. degree in Electronics and Communications Engineering from Alexandria University, Alexandria, Egypt in 2010 and his M.Sc. degree in Microelectronics System Design from Nile University, Cairo, Egypt in 2013. He worked as a Design Engineer for Hittite Microwave Corp., Egypt for 3 years where he designed microwave-integrated circuits using different GaAs and SiGe technologies. He also worked for Analog Devices Inc., Egypt for 2 years performing a similar role. He is currently pursuing his Ph.D. degree at Chalmers University of Technology, Göteborg, Sweden. His research is mainly focused on heterogeneous integration and interconnects for THz systems. His research interests include THz transceivers and their applications.

Dan Kuylenstierna (S'04–M'07) received the M.Sc. degree in Engineering Physics and the Ph.D. degree in Microtechnology and Nanoscience from the Chalmers University of Technology, Göteborg, Sweden, in 2001 and 2007, respectively. He is currently an Associate Professor with the Microwave Electronics Laboratory, Department of Microtechnology and Nanoscience (MC2), Chalmers University. His main scientific interests are MMIC design, reconfigurable circuits, frequency generation, and phase-noise metrology. Dr. Kuylenstierna was the recipient of the IEEE Microwave Theory and Techniques Society (IEEE MTT-S) Graduate Fellowship Award in 2005.

Herbert Zirath received his M.Sc. and Ph.D. degrees from Chalmers University, Göteborg, Sweden, in 1980 and 1986, respectively. He is currently a Professor of High Speed Electronics at the Department of Microtechnology and Nanoscience. He became the Head of the Microwave Electronics Laboratory during 2001, which currently has 70 employees. At present, he is leading a group of approximately 30 researchers in the area of high-frequency semiconductor devices and circuits. His main research interests include InP-HEMT devices and circuits, SiC and GaN-based transistors for high-power applications, device modeling including noise and large-signal models for FET and bipolar devices, and foundry-related MMICs for millimeter-wave applications based on both III-V and silicon devices. He is working part-time at Ericsson AB as a microwave circuit expert. He has authored and co-authored more than 250 papers in international journals and conference proceedings, one book, and holds four patents.

https://doi.org/10.1017/S1759078719000291 Published online by Cambridge University Press